



Experimental and Theoretical Radiative Lifetimes, Branching Fractions, Transition Probabilities, and Oscillator Strengths of Nb I Levels

Yang Gao^{1,4}, Yidan Geng^{1,4}, Pascal Quinet^{2,3}, Xinghao Wang¹, Qi Yu¹, and Zhenwen Dai¹ 

¹ Key Laboratory of Physics and Technology for Advanced Batteries (Ministry of Education), College of Physics, Jilin University, Changchun 130012, People's Republic of China; dai@jlu.edu.cn

² Physique Atomique et Astrophysique, Université de Mons, B-7000 Mons, Belgium

³ IPNAS, Université de Liège, B-4000 Liège, Belgium

Received 2017 July 31; revised 2019 April 15; accepted 2019 April 23; published 2019 June 12

Abstract

Radiative lifetimes for 60 odd-parity levels of Nb I belonging to the $4d^35s5p$ and $4d^45p$ configurations, except for two levels with unknown configuration, which are in the energy range between 23,910.90 and 37,188.28 cm^{-1} , are measured by the time-resolved laser-induced fluorescence technique. The lifetime values range from 7.1 to 118.7 ns with uncertainties less than 10%. To our knowledge, 45 lifetime values determined in this paper are reported for the first time. By combining the experimental lifetimes with measured or computed branching fractions, we obtain transition probabilities and oscillator strengths for the individual channels depopulating the investigated levels.

Key words: atomic data – methods: data analysis – techniques: spectroscopic

Supporting material: machine-readable tables

1. Introduction

The oscillator strengths in the first and second spectra of the transition metals are essential to determination of solar and stellar abundances of these important elements and provide a vital source of information for astrophysicists to analyze interior motion and evolution of stars (Martinson et al. 1973; Holt et al. 2009). By combination of experimental radiative lifetimes of atomic level with branching fractions (BFs) of spontaneous transitions, the oscillator strengths ($\log(gf)$) of corresponding transitions can be reliably deduced.

Niobium (Nb) is a transition element with 2468°C melting point. It is not easy to generate the gas phase of Nb, thus only a few studies on Nb I lifetimes were reported so far. There are only five papers of radiative lifetime studies on the Nb atom. Rudolph & Helbig (1982) measured six Nb I levels between 25,200 and 27,427 cm^{-1} by the time-resolved laser-induced fluorescence (TR-LIF) technique. In the same year, lifetimes of 11 levels ranging from 23,574 to 27,427 cm^{-1} were measured with TR-LIF method by Kwiatkowski et al. (1982), while 50 lifetimes for the levels from 19,624 to 27,975 cm^{-1} were measured by TR-LIF in a hollow cathode atomic beam by Duquette & Lawler (1982). In 1986, Duquette et al. (1986) reported transition probabilities (gA) for 320 lines in Nb I by combining BFs measured using a Fourier transform spectrometer (FTS) with previous radiative lifetimes (Duquette & Lawler 1982). About three decades later, Malcheva et al. (2011) extended previous investigations, and lifetimes of 17 levels between 27,400 and 47,700 cm^{-1} in Nb I were obtained. In 2015, Mukund et al. (2015) reported on Nb I lifetimes for 37 levels belonging to the $4d^35s5p$ and $4d^45p$ configurations between 18,790 and 35,730 cm^{-1} with the results in the range of 12–340 ns by observing TR-LIF. However, radiative lifetimes of a number of Nb I levels have not been measured yet.

In this paper, radiative lifetimes of 60 odd-parity levels of Nb I are measured using the TR-LIF technique. Moreover, these new experimental results are combined with BF measurements deduced from experimental Nb I spectra available at the National Solar Observatory (NSO) or with BF calculations performed using a relativistic Hartree–Fock approach, including core-polarization effects, in order to deduce gA and $\log(gf)$ for all decay channels depopulating the investigated levels.

2. Experimental Setup

Since the experimental setup used for the lifetime measurements has been described in detail in our previous papers (see e.g., Shang et al. 2015), only a brief summary is given here. A 532 nm Q-switched Nd:YAG laser for ablation with pulse energy about 10 mJ was focused on a Nb target sample with 99.95% purity to produce Nb plasma where there were sufficient free atoms in metastable states. This atom/ion-producing technique is efficient and reliable for lifetime measurements (Berzinsh et al. 1997; Dai et al. 2003). An excitation laser was perpendicular to the ablation laser in the vacuum chamber and was horizontally sent through the plasma zone 8–9 mm above the target to excite the Nb atoms to the investigated levels. The excitation laser of 5–7 ns pulse duration was generated by a tunable dye laser (Sirah Cobra-Stretch), which was pumped by another 532 nm Q-switched Nd:YAG laser (Spectra-Physics). Sometimes, in order to extend excitation wavelength, one or two barium borate (BBO) type-I crystal(s) and a stimulated Raman scattering (SRS) cell filled with H_2 of 15 bars were used. The delay time between the excitation and ablation pulses can be tuned by a digital delay generator (SRS Model 535). The fluorescence emitted from excited states was focused by a fused silica lens in the direction perpendicular to the excitation and ablation lasers and was then gathered in a grating monochromator and detected by a photomultiplier tube (PMT, Hamamatsu R3896). The signals from the PMT were finally registered and averaged

⁴ These authors contributed equally to this work.

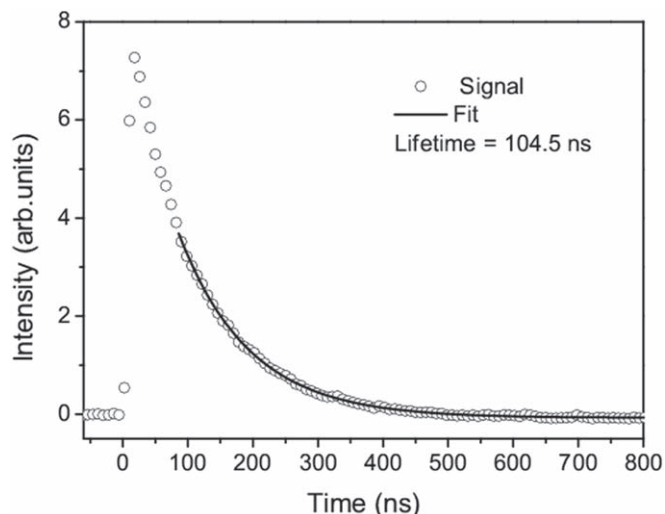


Figure 1. Typical fluorescence decay curve of the $27,797.44 \text{ cm}^{-1}$ Nb I level with an exponential fitting.

by a digital oscilloscope (Tektronix DPO7254). To avoid the affection of excitation laser, some appropriate filters were put in front of the monochromator.

3. Lifetime Measurements

To make sure that only one level was reached at a time, the excitation wavelength needed to be carefully chosen from several available excitation paths, which was monitored by a wavemeter (HighFinesse WS6). Excitation of the target level was confirmed by verifying that all the fluorescence channels were related to this level and that their decay behaviors were the same.

Some systematic effects may bring errors into experimental measurements. Among them, the effects of the flight-out-of-view, PMT nonlinear response, and collision will reduce measured values. On the contrary, the radiation trapping effect may prolong lifetimes. These effects can be eliminated by changing the slit width of the monochromator, reducing the energies of ablation and excitation lasers, and increasing the delay time between the ablation and excitation pulses. Moreover, a magnetic field of about 100 G produced by a pair of Helmholtz coils was applied to wash out possible quantum beats caused by the earth magnetic field and to effectively reduce recombination between electrons and ions (Wang et al. 2014).

In this work, the lifetimes longer than 40 ns were obtained by fitting recorded fluorescence curves to exponential functions. A typical decay curve of the $27,797.44 \text{ cm}^{-1}$ level with an exponential fitting is shown in Figure 1. For the lifetimes shorter than 40 ns, in order to more accurately evaluate lifetime values, deconvolution of fluorescence decay curves are indispensable. For the convolution fitting, the temporal profile of an excitation pulse was registered. A typical fluorescence decay curve of the $29,209.42 \text{ cm}^{-1}$ level with the fitted convolution curve of a laser pulse and an exponential with the decay constant of 19.9 ns is shown in Figure 2. Over 10 fluorescence curves were recorded at different delays for each level, and the final result is the average value of the lifetimes evaluated from these curves.

Natural radiative lifetimes of 60 odd-parity levels of Nb I were measured in this work. They are listed together with the uncertainties in Table 1. In this table, the configurations, terms,

J values, and energies of the levels are from the compilation by Moore (1971). The estimated uncertainties that make up systematic and statistical errors are less than 10%. As can be seen, our results are in good agreement with the results by Duquette & Lawler (1982), Kwiatkowski et al. (1982), and Malcheva et al. (2011). The differences between our measurements and theirs, using ours as the reference, are within 10%.

Slightly larger discrepancies appear when comparing the lifetime values by Mukund et al. (2015) with our results; the average and the root-mean-square differences are 20.6% and 27.2%, respectively. Note that the results of Mukund et al. (2015) are also generally longer than those in other papers (Duquette & Lawler 1982; Kwiatkowski et al. 1982; Malcheva et al. 2011), which is probably because some systematic effects might not be well controlled in the measurements by Mukund et al. (2015).

4. Transition Probability and Oscillator Strength Determination

The theoretical bases for deducing gA and $\log(gf)$ by combining experimental lifetimes and BFs can be found in Jiang et al. (2013). In the present work, we tried to measure BFs for the levels whose lifetimes were measured in Table 1 by observing emission spectrum of an Nb hollow cathode lamp with a grating spectrometer (Acton SpectraPro500i). Unfortunately, we found that almost all the levels have emission lines overlapping with other ones of atomic or ionic niobium so that the BF measurements cannot be performed accurately. However, for 24 among the 60 levels listed in Table 1, it was possible to determine BFs by intensity measurements using the FTS spectra of Nb hollow cathode discharge (HCD) lamps, which are available from the digital library of the National Solar Observatory (NSO) at the Kitt Peak, USA (<http://diglib.nso.edu/>). The other 36 levels cannot be measured because their spectral lines have severe overlaps with other lines of Nb I, II, or III. Table 2 lists the eight FTS spectra from the NSO used for our BF determination in Nb I. Although the spectrum Index 2 has a range from 0 to $36,947 \text{ cm}^{-1}$, the signal-to-noise ratios of spectral lines less than $16,000 \text{ cm}^{-1}$ are so poor that most of the investigated lines cannot be resolved. Similar situations also exist in the spectra Indices 4, 6, and 8. In this case, the spectra of Indices 1, 3, 5, and 7 with higher limits of resolution were used for BF determinations of the lines longer than 600 nm. Thus, we can say that the spectra used for each lamp current involve a red half- and a blue half-spectrum. Note that the currents 209 and 211 mA are considered to be the same when analyzing the two half spectra of Indices 1 and 2.

Since the FTS instrument system has different responses with wavelengths, the recorded spectra should be carefully calibrated based on comparison of the high-precision branching ratios for Ar I and II lines (Hashiguchi & Hasikuni 1985; Whaling et al. 1993) to the intensity ratios measured for the same lines. As each complete spectrum at one discharge current is made up of two half spectra, the calibration curves for the two half spectra at the same current are connected by Ar I and II lines in the overlap region. To examine self-absorption effect on the strong lines, we carefully compared the BF results at different operating currents and found that they are in rather good agreement, which means there is no distinct optical depth effect in the used spectra for the strong lines under investigation.

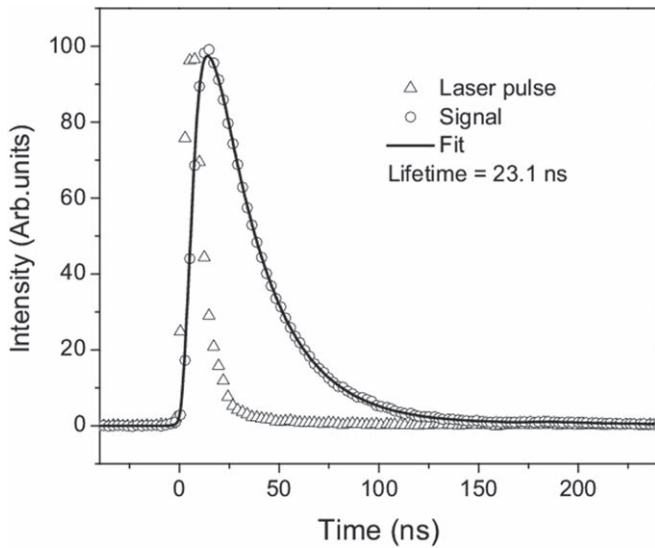


Figure 2. Typical fluorescence decay curve of the 29,209.42 cm⁻¹ Nb I level with a convolution fitting.

Nb has a stable isotope with a larger nuclear spin ($I = 9/2$), and thus many spectral lines exhibit hyperfine structures. In this case, the areas under the line profiles served as line intensities for our determination of BFs. The uncertainties of BF results consist of the line intensity and the calibration errors. The former is an analytical function of the signal-to-noise ratio, the FWHM of the line, and the resolution interval of spectrum, i.e., the step size in a spectrum (Sikström et al. 2002), while the latter was evaluated as 1% per thousand wavenumber separation between the line of interest and the dominant line from the upper level (Wickliffe et al. 2000; Wood et al. 2014). The combined relative uncertainty of BF was calculated as the square root of their quadrature sum (Sikström et al. 2002).

The measured BFs, as well as the deduced experimental gA and $\log(gf)$ values for 255 lines of Nb I, are listed in Table 3. The previous results measured by Duquette et al. (1986) are also presented. The less-than symbols in front of the data mean that the lines may blend with another one. Figure 3 is a comparison of our BFs to the values of Duquette et al. (1986). One can see good agreements for all the results except for two very weak lines, 455.688 nm from 26,936.86 cm⁻¹ and 787.341 nm from 27,596.74 cm⁻¹ with the BFs 0.012 and 0.013, respectively. Note that, for the residual BF of each level, i.e., the sum of BFs corresponding to all the lines not observable in the NSO spectra, we had recourse to theoretical calculations. The latter were performed using the pseudo-relativistic Hartree–Fock (HFR) method developed by Cowan (1981) and modified to take core-polarization effects into account, giving rise to the so-called HFR+CPOL approach (see e.g., Quinet et al. 1999, 2002; Quinet 2017). The physical model was the same as the one considered in the previous theoretical investigation of the niobium atom, as described by Malcheva et al. (2011). As a reminder, 10 even- and nine odd-parity configurations were explicitly included in the model, namely 4d⁵, 4d⁴5s, 4d⁴6s, 4d⁴5d, 4d³5s², 4d³5p², 4d³5d², 4d³5s5d, 4d³5s6s, and 4d²5s5p²; and 4d⁴5p, 4d⁴6p, 4d⁴4f, 4d⁴5f, 4d³5s5p, 4d³5s6p, 4d³5p5d, 4d²5s²5p, and 4d²5p³, respectively. The core-polarization corrections were estimated using the dipole polarizability computed by Fraga et al. (1976) for an Nb IV ionic core ($\alpha_d = 5.80a_0^3$) and a cut-off radius

corresponding to the HFR mean value $\langle r \rangle$ of the outermost 4d core orbital ($r_c = 1.96a_0$). In addition, a semi-empirical fitting procedure was applied to the radial parameters, characterizing the 4d⁵, 4d⁴5s, 4d³5s², 4d⁴5p, and 4d³5s5p configurations in order to reduce the differences between the calculated energy levels and the experimental values given by Kröger et al. (2004, 2007) as much as possible, as described in detail by Malcheva et al. (2011).

In Table 1, the theoretical lifetimes are compared with the experimental values measured in the present work. Although rather large discrepancies subsist for a few levels, an overall agreement between both sets of results is observed, the mean ratio $\tau_{\text{calc}}/\tau_{\text{exp}}$ is found to be equal to 0.92 ± 0.35 when considering all the 60 levels of Table 1. We note that the scattering of results is noticeably reduced when excluding the five levels located at 27,596.74, 27,797.44, 29,209.42, 30,059.60, and 32,213.94 cm⁻¹, for which the differences between calculated and experimental lifetimes exceed a factor of two; the mean ratio, $\tau_{\text{calc}}/\tau_{\text{exp}}$, is equal to 0.93 ± 0.25 in that case.

The same theoretical HFR+CPOL model was used to compute the BFs of the levels for which intensities of spectral lines cannot be estimated accurately in the NSO spectra due to a blending problem. These values, when combined to the experimental lifetimes listed in Table 1, allowed us to provide a new set of semi-empirical gA and $\log(gf)$ values for the 371 spectral lines of neutral niobium listed in Table 4. It is worth mentioning that only transitions for which BF values greater than 1% are given in the table, which leads mostly to transitions with gA values larger than 10^7 s⁻¹. Furthermore, we found that most of the transitions with $gA < 10^7$ s⁻¹ were affected by cancellation effects in our calculations. As a reminder, in order to calculate gA or gf for a transition between the atomic states γJ and $\gamma' J'$, we compute the value of the line strength:

$$S = \langle \gamma J \| P^{(1)} \| \gamma' J' \rangle^2, \quad (1)$$

where $P^{(1)}$ is the electric dipole operator. Because of intermediate coupling and configuration interaction mixing, the wavefunctions are expanded in terms of basis functions:

$$|\gamma J\rangle = \sum_{\beta} y_{\beta J}^{\gamma} |\beta J\rangle, \quad (2)$$

$$|\gamma' J'\rangle = \sum_{\beta'} y_{\beta' J'}^{\gamma'} |\beta' J'\rangle. \quad (3)$$

We may then write Equation (1) in the form

$$S = \left| \sum_{\beta} \sum_{\beta'} y_{\beta J}^{\gamma} \langle \beta J \| P^{(1)} \| \beta' J' \rangle y_{\beta' J'}^{\gamma'} \right|^2. \quad (4)$$

This sum thus represents a mixing of amplitudes rather than line strengths themselves with the consequence that the effect of mixing is not necessarily a tendency to average out the various line strengths. There are frequently destructive interference effects that cause a weak line to become still weaker. In this context, the cancellation factor (CF) is given by

$$\text{CF} = \frac{\left| \sum_{\beta} \sum_{\beta'} y_{\beta J}^{\gamma} \langle \beta J \| P^{(1)} \| \beta' J' \rangle y_{\beta' J'}^{\gamma'} \right|^2}{\sum_{\beta} \sum_{\beta'} |y_{\beta J}^{\gamma} \langle \beta J \| P^{(1)} \| \beta' J' \rangle y_{\beta' J'}^{\gamma'}|^2}. \quad (5)$$

According to Cowan (1981), very small values of this factor (typically when the CF is smaller than about 0.05) indicate that the corresponding transition rates may be expected to show

Table 1
Measured and Calculated Lifetimes for Nb I and Comparison with Previous Results

Config.	Upper Level ^a			$\lambda_{\text{Exc.}}$ (nm)	$\lambda_{\text{Obs.}}$ (nm)	Lifetime (ns)		
	Term	J	E (cm ⁻¹)			This Expt.	Prev. Expt.	This Calc. ^b
4d ⁴ 5p	z ² S ^o	1/2	23910.90	657.653	420.9	81.5(67)	71.5(31) ^c	56.6
4d ³ 5s5p	z ⁴ F ^o	9/2	24506.53	637.774	460.8	35.8(15)	37.7(7) ^c , 35.9(18) ^d , 33.2(17) ^e	33.1
4d ⁴ 5p	y ⁴ D ^o	3/2	26936.86	371.239	394.5	23.0(7)	22.1(11) ^d	11.5
4d ⁴ 5p	X ⁶ D ^o	7/2	27427.07	641.230	395.7	7.5(3)	7.7(4) ^d	10.3
4d ³ 5s5p	y ⁴ P ^o	1/2	27498.94	363.650	379.4	20.6(10)	22.9(11) ^c	14.6
4d ⁴ 5p	y ⁴ D ^o	7/2	27596.74	367.583	393.0	29.1(14)	31.9(16) ^d	12.4
	276 ^o	5/2	27614.10	364.167	384.2	93.9(65)	101.0(50) ^c	53.0
4d ³ 5s5p	x ⁴ D ^o	1/2	27666.46	361.448	441.1	17.5(6)	22.4(21) ^c	18.8
4d ³ 5s5p	z ² F ^o	5/2	27797.44	364.891	390.0	104.5(33)	...	38.8
4d ³ 5s5p	y ² G ^o	7/2	27855.13	368.190	399.2	112.1(83)	...	102.1
	z ² P ^o	3/2	27918.85	360.170	436.3	21.5(12)	29.3(18) ^c	16.2
4d ⁴ 5p	x ⁶ D ^o	9/2	27974.87	366.574	371.4	11.4(3)	10.8(6) ^d	7.9
4d ⁴ 5p	z ⁴ S ^o	3/2	28208.48	359.499	449.6	8.6(4)	12.3(6) ^c	5.0
	z ² P ^o	1/2	28442.16	366.309	351.6	59.7(27)	66.1(44) ^c	41.0
4d ³ 5s5p	x ⁴ D ^o	7/2	29209.42	369.613	430.2	23.1(7)	30.7(17) ^c	11.1
4d ³ 5s5p	z ⁴ H ^o	7/2	29271.99	368.76	429.1	59.3(41)	...	71.9
4d ³ 5s5p	z ⁴ H ^o	9/2	29519.05	365.431	374.3	102.9(64)	...	78.9
4d ³ 5s5p	z ⁶ S ^o	5/2	30059.60	358.352	471.0	118.7(96)	...	304.5
4d ⁴ 5p	x ⁴ F ^o	9/2	30279.23	363.982	481.2	27.6(6)	...	29.2
4d ³ 5s5p	y ⁴ S ^o	3/2	31174.65	322.368	382.0	10.4(5)	...	10.5
4d ³ 5s5p	x ² G ^o	7/2	31800.74	318.487	435.3	45.5(42)	...	23.4
4d ⁴ 5p	v ⁴ F ^o	5/2	31807.55	315.922	330.9	17.9(11)	...	17.2
4d ⁴ 5p	u ⁴ F ^o	3/2	31907.74	371.615	313.4	13.0(6)	...	14.4
4d ³ 5s5p	w ⁴ F ^o	5/2	32013.40	316.241	334.9	24.9(13)	...	15.4
4d ⁴ 5p	w ⁴ D ^o	1/2	32066.06	369.441	442.0	15.9(7)	...	18.4
4d ⁴ 5p	z ⁴ I ^o	9/2	32156.00	321.484	424.7	18.6(11)	...	24.0
4d ³ 5s5p	x ² G ^o	9/2	32213.94	320.886	437.0	32.2(14)	46.2(27) ^c	12.6
4d ⁴ 5p	w ⁴ D ^o	3/2	32248.69	366.965	424.7	16.5(8)	...	16.1
4d ³ 5s5p	w ⁴ F ^o	7/2	32333.18	316.076	338.7	12.3(2)	...	10.7
4d ⁴ (² 5p)	z ⁴ I ^o	11/2	32382.24	319.63	468.6	27.3(13)	...	20.5
4d ⁴ 5p	u ⁴ F ^o	7/2	32451.99	314.894	419.5	16.2(9)	...	23.4
4d ⁴ 5p	w ⁴ D ^o	5/2	32545.52	367.005	425.5	19.9(9)	...	18.4
4d ⁴ 5p	v ⁴ F ^o	9/2	32605.39	316.906	420.6	8.3(5)	...	11.7
4d ³ 5s5p	x ² D ^o	3/2	32623.02	365.964	444.5	12.6(13)	...	15.9
4d ⁴ 5p	v ² F ^o	5/2	32654.48	365.543	423.5	14.9(5)	...	11.5
4d ⁴ 5p	w ⁴ G ^o	9/2	32802.44	314.939	417.1	44.5(43)	41.1(30) ^f	47.1
4d ⁴ 5p	v ² F ^o	7/2	32899.08	371.283	424.3	14.5(7)	...	20.4
4d ³ 5s5p	w ⁴ F ^o	9/2	32923.87	313.739	423.8	32.6(13)	...	19.7
4d ⁴ 5p	w ⁴ D ^o	7/2	33003.89	369.844	313.0	19.5(15)	...	10.4
4d ³ 5s5p	w ² D ^o	3/2	33086.98	368.711	435.5	25.9(11)	...	20.4
4d ⁴ 5p	u ⁴ F ^o	9/2	33136.30	322.766	420.0	9.0(8)	...	9.1
4d ³ 5s5p	w ² D ^o	5/2	33389.87	320.146	418.5	22.3(14)	...	18.6
4d ³ 5s5p	z ² I ^o	11/2	34004.08	320.526	444.9	15.2(8)	...	13.6
4d ³ 5s5p	w ² G ^o	9/2	34235.04	311.712	431.2	47.2(46)	...	24.6
4d ³ 5s5p	y ² P ^o	3/2	34252.96	306.128	416.4	20.2(8)	...	29.3
4d ³ 5s5p	w ² G ^o	7/2	34319.09	317.322	429.6	45.5(27)	...	34.0
4d ⁴ 5p	z ² H ^o	9/2	34415.52	316.354	427.9	16.9(10)	...	22.6
4d ³ 5s5p	x ⁴ P ^o	5/2	34703.70	307.224	389.7	7.5(5)	...	6.5
4d ⁴ 5p	z ² H ^o	11/2	34838.33	312.178	392.0	17.1(15)	...	16.9
4d ⁴ 5p	v ⁴ G ^o	7/2	34853.50	312.031	432.9	18.4(5)	...	18.6
4d ⁴ 5p	v ⁴ G ^o	9/2	35156.94	309.104	389.7	16.0(9)	...	16.4
4d ³ 5s5p	u ² F ^o	7/2	35178.82	308.895	389.4	25.1(13)	...	26.0
4d ⁴ 5p	y ² H ^o	11/2	35344.86	307.319	415.0	16.6(6)	...	17.6
4d ⁴ 5p	y ² H ^o	9/2	35496.39	305.894	412.0	16.5(5)	...	15.1
4d ⁴ 5p	u ² D ^o	3/2	35829.46	324.346	432.2	20.4(8)	...	15.3
4d ⁴ 5p	u ⁴ D ^o	1/2	35920.45	323.91	406.5	7.1(4)	...	6.1
4d ⁴ 5p	u ⁴ D ^o	5/2	36180.13	323.811	418.6	9.0(5)	...	6.6
4d ⁴ 5p	s ² F ^o	5/2	36866.60	323.613	391.4	8.4(5)	...	8.6
4d ⁴ 5p	t ⁴ F ^o	3/2	37111.67	311.396	398.5	12.2(5)	...	14.6
4d ⁴ 5p	u ⁴ G ^o	5/2	37188.28	313.574	408.2	8.0(3)	...	8.7

Notes.^a Moore (1971).^b HFR+CPOL calculations (see the text).^c Mukund et al. (2015).^d Duquette & Lawler (1982).^e Kwiatkowski et al. (1982).^f Malcheva et al. (2011).

Table 2
FTS of Nb HCD Lamps Used in This Study

Index	Date	Serial Number	Buffer Gas and Pressure (Torr)	Lamp Current (mA)	Wavenumber Range (cm ⁻¹)	Limit of Resolution (cm ⁻¹)	Co-adds	Beam Splitter	Filter
1	1984 Mar 19	2	Ar 0.4	209	0–22831	0.033	8	UV	...
2	1984 Mar 19	1	Ar 0.5	211	0–36947	0.053	8	UV	...
3	1984 Mar 19	3	Ar 0.3	101	0–22831	0.033	8	UV	...
4	1984 Mar 19	4	Ar 0.3	101	14432–36081	0.053	8	UV	CuSO ₄
5	1984 Mar 19	6	Ar 0.3	51	7491–22028	0.033	8	UV	GG495
6	1984 Mar 19	5	Ar 0.3	51	14432–36081	0.053	8	UV	CuSO ₄
7	1984 Mar 19	7	Ar 0.3	23	7491–22028	0.033	8	UV	GG495
8	1984 Mar 19	8	Ar 0.3	23	14432–36081	0.053	9	UV	CuSO ₄

Note. All the FTS spectral data are publicly available at <http://Diglib.Nso.Edu/>.

Table 3
Experimental Transition Probabilities (gA_{exp}) and Oscillator Strengths ($\log(gf_{\text{exp}})$) for the Nb I Levels for which the Lifetimes Have Been Measured in the Present Work and for which the Branching Fractions (BF_{exp}) Have Been Deduced from Line Intensity Measurements on NSO Spectra

Upper Level ^a			$\tau(\text{ns})$	Lower Level ^a		$\lambda_{\text{air}} (\text{nm})$	$\text{BF}_{\text{exp}}(\%)$		$gA_{\text{exp}}(10^6 \text{ s}^{-1})$		$\log(gf_{\text{exp}})$		$gA_{\text{calc}} (10^6 \text{ s}^{-1})$ This Work
Config.	J	$E_k(\text{cm}^{-1})$		J	$E_i (\text{cm}^{-1})$		This Work	Previous ^b	This Work	Previous ^b	This Work	Previous ^b	
4d ⁴ 5p	1/2	23910.90	81.5(67)	1/2	0.00	418.102	1.4(4)		0.348(106)		-3.04(13)		3.30
				3/2	154.19	420.815	29.9(18)		7.34(74)		-1.71(4)		2.95
				3/2	1142.79	439.087	0.2(1)		0.043(33)		-3.91(33)		0.14
				1/2	4998.17	528.597	0.7(2)		0.169(41)		-3.15(11)		0.03
				3/2	5297.92	537.110	5.5(5)		1.34(16)		-2.24(5)		0.59
				1/2	8410.90	644.983	4.4(6)		1.09(16)		-2.17(7)		0.15
				1/2	8705.32	657.472	6.4(7)		1.56(22)		-1.99(6)		0.94
				1/2	9439.08	690.808	14.2(14)		3.48(46)		-1.60(6)		5.15
				1/2	10126.06	725.235	24.1(23)		5.92(75)		-1.33(6)		7.38
				3/2	11318.09	793.886	12.9(39)		3.17(100)		-1.52(14)		3.63
							[0.3]						

Notes. In the BF column, the values between brackets correspond to residual BFs estimated using HFR+CPOL calculations (see the text). For the levels with previous results, the residual BFs are not given in order to make direct comparisons. In the last column, the HFR+CPOL gA values (gA_{calc}) are also given for comparison.

^a Moore (1971).

^b Duquette et al. (1986).

(This table is available in its entirety in machine-readable form.)

Table 4

Semi-empirical Transition Probabilities (gA_{calc}) and Oscillator Strengths ($\log(gf)_{\text{calc}}$) for the Strongest Decay Channels Depopulating the Nb I Levels for which the Lifetimes Have Been Measured in the Present Work and for which the Branching Fractions (BF_{calc}) Have Been Computed Using the Theoretical HFR+CPOL Method

Upper Level	Lower Level	$\lambda(\text{nm})$	$\text{BF}_{\text{calc}}^{\text{a}}$ (%)	$gA_{\text{calc}}^{\text{b}}$ (s^{-1})	$\text{Log}(gf)_{\text{calc}}^{\text{b}}$	Note ^c
27797.44 (o) 5/2	154.19 (e) 3/2	361.649	24.6	1.41E+07	-1.56	
$\tau = 104.5(33)$ ns	391.99 (e) 5/2	364.787	5.2	3.00E+06	-2.22	
	695.25 (e) 7/2	368.869	22.4	1.29E+07	-1.58	
	1142.79 (e) 3/2	375.062	4.8	2.75E+06	-2.24	
	2154.11 (e) 7/2	389.855	18.4	1.06E+07	-1.62	
	5965.45 (e) 5/2	457.915	1.4	8.30E+05	-2.58	*
	8705.32 (e) 3/2	523.631	4.4	2.55E+06	-1.98	
	8827.00 (e) 7/2	526.989	6.9	3.98E+06	-1.78	*
	9043.14 (e) 5/2	533.063	3.9	2.22E+06	-2.02	*
	13404.77 (e) 5/2	694.607	1.8	1.04E+06	-2.12	*

Notes.

^a Calculated using the HFR+CPOL method (see the text). Only transitions with $\text{BF} > 1\%$ are given.

^b Deduced from the combination of theoretical branching fractions and experimental radiative lifetimes of Table 1. The estimated uncertainties are 50% for transitions with gA values larger than 10^8 s^{-1} and within a factor of two for weaker transitions, which corresponds to 0.2 and 0.3 dex on the $\log(gf)$ scale, respectively.

^c Transitions marked with an asterisk (*) are those for which the cancellation factors were found to be smaller than 0.05 (see the text).

(This table is available in its entirety in machine-readable form.)

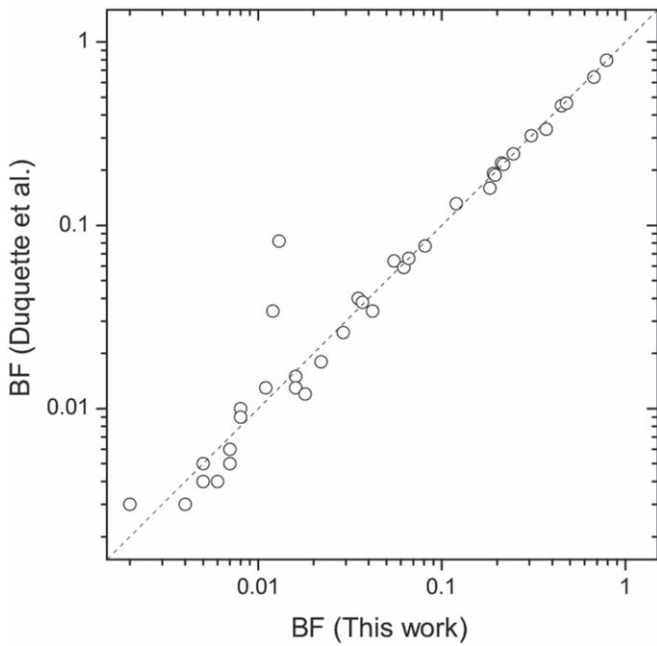


Figure 3. Comparison of our BF results with those of Duquette et al. (1986). The dashed line marks the equality.

large percentage errors. In Figure 4, CF factors are plotted as a function of gA values for all Nb I transitions. As seen from this figure, it is clear that most of the lines with gA smaller than 10^7 s^{-1} are affected by very small values of the CF, indicating that the corresponding decay rates could be unreliable. On the contrary, most of the transitions listed in Table 4, in particular those with $gA > 10^8 \text{ s}^{-1}$, do not appear to be affected by cancellation effects. Note that the transitions for which the CF were found to be smaller than 0.05 are indicated in Table 4.

In order to estimate the uncertainties related to the theoretical results, we compared our calculated gA values ($gA > 10^6 \text{ s}^{-1}$) to the experimental data obtained in the present work. Such a comparison is given in Table 3 and is shown in Figure 5. As we found that, for a large majority of lines with gA values larger

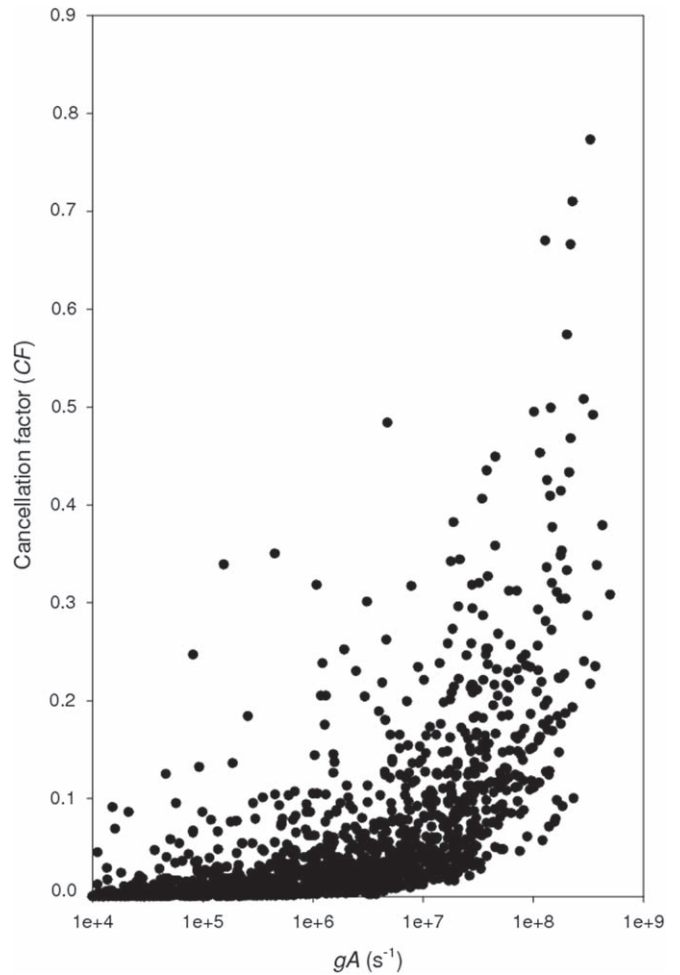


Figure 4. Cancellation factors plotted as a function of gA values, as obtained in the present HFR calculations for Nb I spectral lines.

(smaller) than 10^8 s^{-1} , both sets of results presented a general agreement within 50% (a factor of two); these latter values were chosen as an overall estimation of the errors affecting the transition probabilities and oscillator strengths listed in Table 4.

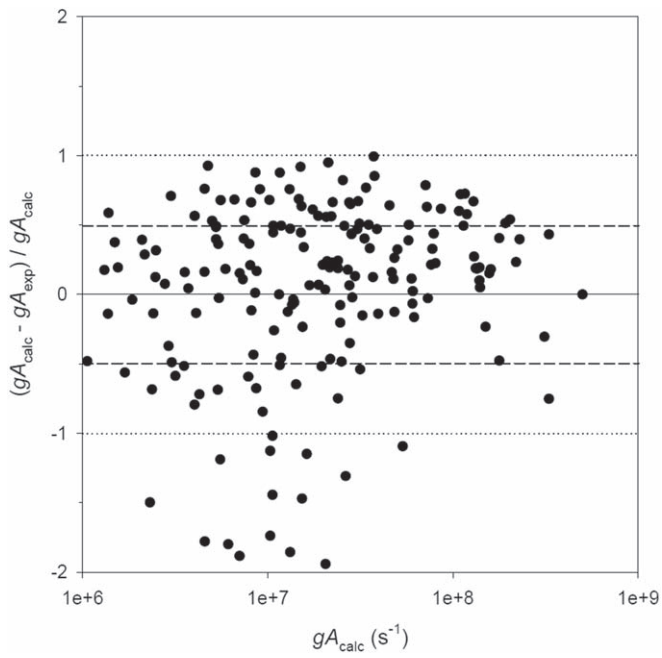


Figure 5. Comparison between the experimental and calculated transition probabilities obtained in the present work. The dashed and dotted lines correspond to relative differences of 50% and a factor of two, respectively.

This work was supported by the National Natural Science Foundation of China (grant No. U1832114) and the Science and Technology Development Planning Project of Jilin Province (grant No. 20180101239JC). P.Q. is the Research Director of the Belgian F.R.S.-FNRS from which financial support is gratefully acknowledged.

ORCID iDs

Zhenwen Dai  <https://orcid.org/0000-0002-9040-2315>

References

- Berzinsh, U., Caiyan, L., Zerne, R., Svanberg, S., & Biémont, É. 1997, *PhRvA*, **55**, 1836
- Cowan, R. D. 1981, *The Theory of Atomic Structure and Spectra* (Berkeley, CA: Univ. California Press)
- Dai, Z. W., Jiang, Z. K., Xu, H. L., et al. 2003, *JPhB*, **36**, 479
- Duquette, D. W., Den Hartog, E. A., & Lawler, J. E. 1986, *JQRST*, **35**, 281
- Duquette, D. W., & Lawler, J. E. 1982, *PhRvA*, **26**, 330
- Fraga, S., Karwowski, J., & Saxena, K. M. S. 1976, *Handbook of Atomic Data* (Amsterdam: Elsevier)
- Hashiguchi, S., & Hasikuni, M. 1985, *JPSJ*, **54**, 1290
- Holt, R. A., Li, R., Chatelain, R., et al. 2009, *PhyS*, **134**, 014012
- Jiang, L. Y., Wang, Q., Shang, X., et al. 2013, *JOSAB*, **30**, 489
- Kröger, S., Öztürk, I. K., Acar, F. G., et al. 2007, *EPJD*, **41**, 61
- Kröger, S., Scharf, O., Guthöhrlein, G., et al. 2004, *EPL*, **344**, 349
- Kwiatkowski, M., Zimmermann, P., Biémont, E., & Grevesse, N. 1982, *A&A*, **112**, 337
- Malcheva, G., Nilsson, H., Engström, L., et al. 2011, *MNRAS*, **412**, 1823
- Martinson, I., Curtis, L. J., Brzozowski, J., & Buchta, R. 1973, *PhyS*, **8**, 62
- Moore, C. E. 1971, *Atomic Energy Levels, As Derived from the Analysis of Optical Spectra: NSRDS-NBS 35, Vol. II* (Washington, DC: NBS)
- Mukund, S., Bhattacharyya, S., Yarlagadda, S., & Nakhate, S. G. 2015, *JQRST*, **166**, 68
- Quinet, P. 2017, *CaJPh*, **95**, 790
- Quinet, P., Palmeri, P., Biémont, E., et al. 1999, *MNRAS*, **307**, 934
- Quinet, P., Palmeri, P., Biémont, E., et al. 2002, *JAJIC*, **344**, 255
- Rudolph, J., & Helbig, V. 1982, *PhLA*, **89**, 339
- Shang, X., Wang, Q., Zhang, F. F., Wang, C., & Dai, Z. W. 2015, *JQRST*, **163**, 34
- Sikström, C. M., Nilsson, H., Litzén, U., Blom, A., & Lundberg, H. 2002, *JQRST*, **74**, 355
- Wang, Q., Jiang, L. Y., Quinet, P., et al. 2014, *ApJS*, **211**, 31
- Whaling, W., Carle, M. T., & Piti, M. L. 1993, *JQRST*, **50**, 7
- Wickliffe, M. E., Lawler, J. E., & Nave, G. 2000, *JQRST*, **66**, 363
- Wood, M. P., Lawler, J. E., Sneden, C., & Cowan, J. J. 2014, *ApJS*, **211**, 20